American Mineralogist, Volume 77, pages 534–544, 1992

Microdistribution of Al, Li, and Na in α quartz: Possible causes and correlation with short-lived cathodoluminescence

Beat Perny, Peter Eberhardt
Physikalisches Institut, Sidlerstrasse 5, Universität Bern, 3012 Bern, Switzerland
Karl Ramseyer
Geologisches Institut, Baltzerstrasse 1, Universität Bern, 3012 Bern, Switzerland
Josef Mullis
Mineralogisches Institut, Bernoullistrasse 30, Universität Basel, 4056 Basel, Switzerland
Rainer Pankrath*
Institut für Mineralogie und Kristallographie der Ruhr-Universität Bochum, Universitätsstraße 150, D-4630 Bochum, Germany

Abstract

The distribution of Al, Li, and Na in natural quartz crystals has been measured by secondary ion mass spectrometry in individual growth layers identified by cathodoluminescence and artificial γ irradiation. Changes of trace element concentrations by more than 3 orders of magnitude were observed on a scale of a few tens of micrometers. The Li and Al abundances are well correlated, and a similar concentration trend may exist for Na. The variability of trace elements in one crystal exceeds the concentration range observed for bulk crystals from all regions of the Swiss Alps.

Zones with intensive, short-lived blue luminescence contain the highest Al and Li concentrations of up to 10000 atoms per 10^6 Si atoms (ppma), whereas nonluminescent regions show the lowest concentrations, <5 ppma. This high variability in trace element concentration is growth related and reflects fluctuations of temperature, pressure, pH, and composition of the fluids during growth. Hydrothermal experiments and theoretical calculations imply that the most likely explanation of these drastic variations in the trace element concentration at a microscopic scale may be changes in pH.

Introduction

Substitutional and interstitial incorporation of trace elements like Al, Fe, Ti, P, H, Li, Na, or K in natural hydrothermally formed quartz crystals is well known (e.g., Bambauer, 1961; Dennen, 1966; Smith and Steele, 1984), but their growth-related distribution is poorly defined (Bambauer, 1961; Poty, 1969; Hervig and Peacock, 1989). Heterogeneous incorporation of trace elements in growth zones is the result of variations in the physico-chemical growth conditions through time (Lehmann and Bambauer, 1973; Harrison et al., 1988; Ramseyer and Mullis, 1990). Knowledge of the growth-related changes in the trace element content is therefore essential for deciphering changes in temperature, pressure, pH, and composition of the fluid during crystal growth. In addition, the determination of the trace element distribution pattern may help to resolve the origin of the observed short-lived cathodoluminescence colors (a few tens of seconds; Ramseyer et al., 1988; Ramseyer and Mullis, 1990).

The prevailing impurities in natural colorless and smoky quartz are Al, H, Li, and Na (Lehmann and Bambauer, 1973; Cohen, 1985), with Al^{3+} substituting for Si^{4+} in the Si-O tetrahedra and H^+, Li^+, and Na^+ acting as charge compensator ions situated at interstitial positions in channels parallel to the c axis (Lehmann and Bambauer, 1973; Jain and Nowick, 1982; Siebers, 1986). Amethyst and rose quartz may contain in addition hundreds of ppma of Fe and Ti (1 ppma is defined as the number of atoms of the element in a total of 10^6 Si atoms).

Different methods have been used to determine the trace concentrations in natural quartz crystals (e.g., AAS, ICP, VIS and IR spectroscopy, electron microprobe), but the measurements have been made either on entire crystals assuming a homogeneous trace element distribution (Cohen, 1960; Kats et al., 1962; Smith and Steele, 1984; Kronenberg et al., 1986) or on specific regions of large crystals (Bambauer, 1961; Bambauer et al., 1961; Poty, 1969; Pankrath, 1988). Quantitative in situ trace element determination in domains of a few micrometers at the ppma level has become feasible by secondary ion mass spectrometry (SIMS; Shimizu et al., 1978; Steele et al., 1981; Rovetta et al., 1989; Hervig and Peacock, 1989).

The aims of this work were (1) to determine the trace

* Present address: Universität Osnabrück, Fachbereich Physik, Barbarastraße 7, 4500 Osnabrück, Germany.

0003–004X/92/0506–0534$02.00

element distribution in zoned natural quartz crystals on a microscopic scale, (2) to search for correlations between the short-lived blue cathodoluminescence and the trace elements Al, Li, and Na, and (3) to unravel the possible causes of the high variability in trace element content. Two natural hydrothermal quartz crystals from the Swiss Alps were selected to cover different growth conditions (Bambauer, 1961; Mullis, 1987; Ramseyer and Mullis, 1990). A detailed description of the two quartz crystals is given in Appendix 1.

Experimental procedures

Sample preparation

The quartz crystals were cut either perpendicular or parallel to the optical **c** axis and then prepared as petrographic thick sections. To avoid possible surface contamination, only diamond was used for final grinding and polishing of the samples. For cleaning, the samples were then wiped with a soft fiber-free cloth and pure alcohol, soaked in diluted nitric acid (≈30%) for 10–15 min at room temperature, and finally rinsed several times in doubly distilled H_2O. After drying at room temperature, the sample was coated with an ≈40 nm Au layer. For electron microprobe analysis an additional C coat was applied after the SIMS analysis. The transparency of the C layer enabled analysis at the same position as used by SIMS.

Artificial γ irradiation

Prior to the cathodoluminescence observations and SIMS measurements, both samples were subjected to artificial γ irradiation from a ^{60}Co source (dose = 40 Mrad, t = 43 h, $T \approx 20$ °C).

Cathodoluminescence observations

The luminescence colors of the quartz samples were studied using a high-sensitivity cathodoluminescence microscope (Ramseyer et al., 1989). The samples were bombarded with electrons (30 keV) at a beam-current density of 0.4 μA/mm². Color slides of the luminescence features were taken with Ektachrome 400 color transparency film and developed at 800 ASA. The exposure time was 100 s. The spectral response of the luminescence was recorded between 370 and 750 nm with 10 nm resolution using a PTI series 001 monochromator equipped with a Hamamatsu R928 photomultiplier.

Electron microprobe determinations

An ARL-SEMQ electron microprobe was used to measure the trace Al content in quartz with the wavelength dispersive system (TAP-crystal). The operating conditions were a beam energy of 15 keV, sample current of 20 nA, and counting time of 100 s. The Al concentrations are based on albite as standard and were corrected for effects of atomic number, absorption, and fluorescence (ZAF correction). The detection limit for Al in quartz (3σ error) was found to be 50 ppm (111 ppma).

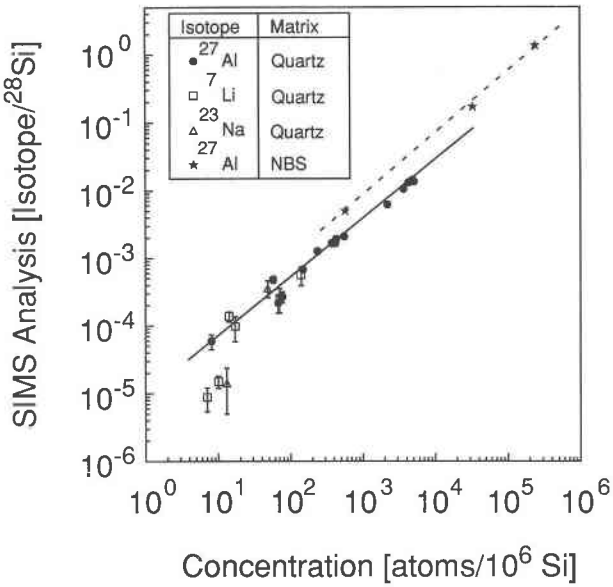

Fig. 1. SIMS calibration curve for Al, Li, and Na. Ion intensities are reported relative to ^{28}Si. Solid line: logarithmic fit including only Al values on quartz samples. Dashed line: logarithmic fit through the three Al values from NBS glass samples. Elemental concentrations are those obtained from AAS and electron microprobe. Error bars represent range of measured (isotope/^{28}Si) ratios.

SIMS measurements

The measurements were carried out with a Cameca-IMS3f instrument. The vacuum in the sample chamber during analysis was maintained at ≈5 × 10^{-6} Pa. A primary $^{16}O^-$ beam of <20 nA with a net energy of 12.5 keV was focused onto a spot of ≈20-μm diameter and rastered over an area of 50 × 50 μm². Only the secondary ions emanating from a 10-μm spot in the center of the rastered area were collected (transfer optics = 150 μm, field aperture = 100 μm, contrast aperture = 400 μm). Positive secondary ions were extracted at −4.5 keV to the ground potential through an energy window of 50 eV without any offset.

These operating parameters are necessary to obtain (1) no crater edge effects, (2) a high current density and small raster size for best sensitivity (low detection limit), (3) a minimal and stable sample charge-build-up, and (4) a reasonable collection time for one analysis.

After selecting a position to analyze, the area was presputtered with the rastered primary beam for 5–20 min to remove the Au layer and any surface contaminations and to obtain stable currents for $^{28}Si^+$, $^7Li^+$, $^{23}Na^+$, and $^{27}Al^+$. Sample charging of −10 to −40 V was compensated by adjustment of the accelerating voltage.

Electromigration caused by charging might be expected (Hughes et al., 1972; Wilson et al., 1989). By using the imaging system on the IMS3f, the diffusion of $^{23}Na^+$ could be observed when the primary current density was increased above the value used for the analysis. In view of the reproducibility of the results and the low sample

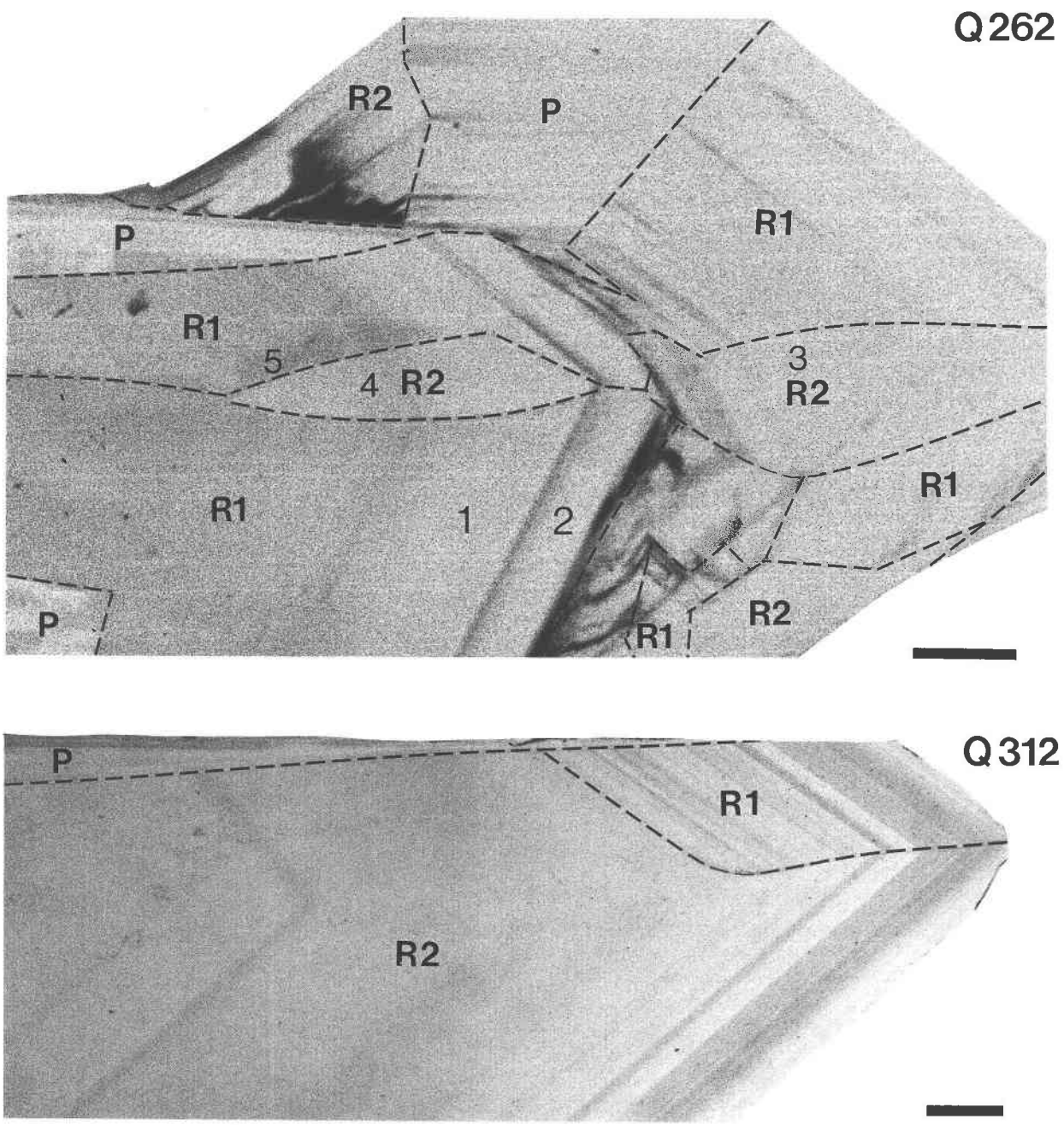

Fig. 2. Quartz samples Q262 and Q312 with smoky color induced by γ irradiation. Areas with growth normal to the prism (P) and positive and negative rhombohedra (R1, R2) are indicated. Numbers (1, 2, 3) represent zones of similar coloring by γ irradiation but with significant different trace element concentrations (Table 1). Zones 4 and 5 have different coloring but similar trace element concentration. Scale bar is 500 μm.

→

Fig. 3. Cathodoluminescence photograph of sample Q262 (**a**) and Q312 (**b**) after γ irradiation. (**c**) Q312 after annealing at 400 °C for 72 h. The points measured in the line scan analyses are marked in the profiles P1, P2, P3, and P4. Zones have been classified according to their characteristic luminescence color (see Table 1). Scale bar is 500 μm.

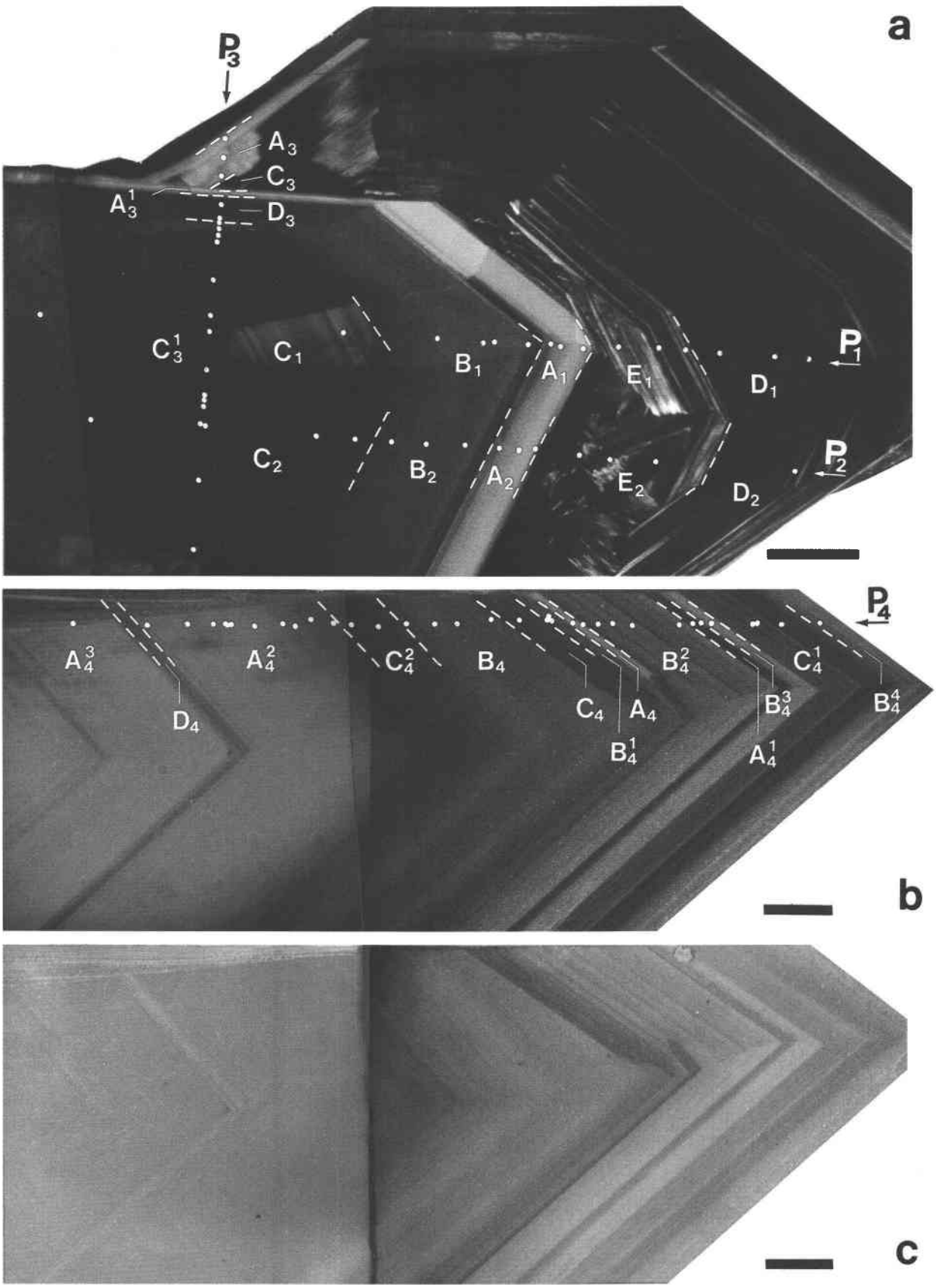
a
P3
A3
C3
D3
A13
C13
C1
B1
A1
E1
D1
P1
C2
B2
A2
E2
D2
P2
b
P4
A43
A42
C42
B4
B42
C41
D4
C4
A4
B43
B44
B41
A41
c

charging, we assume that our depth profiles are not influenced significantly by field-enhanced migration of mobile species. However, slight initial increase in $^{7}Li^{+}$ and a substantial decrease in $^{23}Na^{+}$ intensity with time have been observed in most measurements. The decrease in $^{23}Na^{+}$ intensity can probably be better explained by residual surface contamination than by electromigration. The $^{7}Li^{+}$ increase might be due to Li-H exchange close to the surface during the cleaning with nitric acid. Another explanation may be changes in the sputtering yield from topographic irregularities due to the sputtering process (Stevie and Kahora, 1987).

The statistical counting errors for the measurements are about 1–4% for $^{27}Al/^{28}Si$, 4–10% for $^{7}Li/^{28}Si$, and 10–50% for $^{23}Na/^{28}Si$. Repeat measurements performed during short time intervals without changing samples or readjusting instrument parameters (e.g., during 1 d) agree within these error limits. However, the major contribution to the total analytical uncertainty is due to changes in instrument sensitivity after sample change and complete readjustment of all instrumental parameters between different measuring periods. Furthermore, the limited reproducibility of the beam positioning and the large concentration gradients in some samples lead to additional uncertainties. The overall reproducibility of the results has been checked by multiple analysis of several positions during six months.

To avoid contamination of the sample chamber a Si wafer was used instead of the standard Cameca Cu-on-Al grid for the daily adjustments of the instrument. No sufficiently pure synthetic quartz sample was available as test target for background determination. However, the lowest count rates observed at some positions of the Q262 and Q312 samples corresponded to <0.3 ppma ^{7}Li, <0.1 ppma ^{23}Na, and <3 ppma ^{27}Al. We use these concentrations as upper limits for the background and as detection limits.

The H background of the instrument made measurements of H concentrations in the ppma level impossible (Yurimoto et al., 1989; Magee and Botnick, 1981).

In spite of sophisticated theoretical models for the ionization process (Benninghoven et al., 1987, and references therein), trace element quantification from SIMS data is not yet possible without using standard samples of almost identical composition and crystal structure (Ray and Hart, 1982; Williams, 1985, 1987). We had only six synthetic quartz samples available with known trace element concentrations, all <140 ppma (see Appendix 1). The homogeneity of the trace element distribution in the synthetic quartz samples is not known. To enlarge this very limited standard base, we determined the Al/Si elemental ratio with an electron microprobe at selected points along the profiles measured by SIMS in the natural quartz crystal Q262. Three NBS glass standards were used to extend the calibration to higher concentrations.

The results are shown in Figure 1. The spread of the SIMS results on the synthetic quartz samples might well reflect heterogeneities within these samples. The ^{27}Al data on the quartz define, in the log-log representation, an essentially linear correlation that can be approximated by ($r = 0.98$):

$$\log c_x = 1.16 \log(^{27}Al/^{28}Si) + 5.85$$

where c_x is the elemental concentration in units of ppma. Three NBS glass standards also show a linear dependence with approximately the same slope but clearly offset. This is in agreement with the conclusion reached by Ray and Hart (1982) that glass standards cannot be used for trace element analysis of crystals.

The available limited calibration data for ^{7}Li and ^{23}Na agree with the ^{27}Al measurements except for the three samples with the lowest concentrations. The concentrations in these samples were close to or at the blank and detection limit of the method used (AAS), and the chemical abundances reported may be erroneously high. We therefore disregard these three samples and use for ^{7}Li and ^{23}Na the same calibration curve as for ^{27}Al.

It is important to point out that the conclusions reached by the present study are not influenced by the uncertainties in the calibration curves at the lowest concentrations. The study is based on relative variations, and most of the measured concentrations exceed 10 ppma.

Experimental results

Artificial γ irradiation generated a complex pattern of smoky colored zones in the two crystals (Fig. 2). The orientation of these zones is mostly parallel to the crystal faces.

Cathodoluminescence of both crystals following γ irradiation is shown in Figures 3a and 3b. The macroscopic morphology is identical to the pattern generated by artificial γ irradiation, but the microstructure is better visible under cathodoluminescence. It has to be taken into account that the luminescence is observed through the crystal (Ramseyer et al., 1989) and therefore a lower luminescence intensity will be observed in smoky colored zones because of an absorption band at 2.85 eV (435 nm; see Schirmer, 1976; Nassau and Prescott, 1975). According to the luminescence pattern of the γ-irradiated crystals, five characteristic zones are distinguished (A–E, see Table 1).

Under luminescence, Q262 (Fig. 3a) reveals a complex growth history, with a prismatic dark core followed by an intense blue luminescing layer (zones A_1, A_2, Fig. 3a). At the beginning (prismatic core), the growth was continuous but changed as a result of tectonic activity to a discontinuous crystallization (Mullis, 1976). A dramatic decrease of the fluid pressure from a lithostatic value (180–140 MPa) toward a hydrostatic value (47–44 MPa) caused rapid precipitation of SiO_2 (zones E_1, E_2, D_1, and D_2; for more details see Mullis, 1976). In contrast to the slowly growing central part of the crystal, where the growth is preferentially normal to the rhombohedra (r $\{10\bar{1}1\}$, z $\{01\bar{1}1\}$), the growth in the rapidly precipitated part is normal to the rhombohedra as well as to the prism (m

TABLE 1. Trace element content (ppma) for the different zones of cathodoluminescence color

Luminescence color	Zone	Q262			Q312		
		Al	Li	Na	Al	Li	Na
Strong blue	A	6000–8000	3000–8000	<5–180	150–1200	30–350	<5–20
Blue-gray	B	60–450	40–350	<5	100–250	20–50	<5
Dark gray	C	400–850	250–500	<10	100–500	20–50	<5
Nonluminescent	D	<5	<5	<5	—	—	—
Heterogeneous	E	5–150	<5–150	<5	—	—	—

$\{10\bar{1}0\}$). The rapidly grown part of the crystal shows at the beginning a complex luminescence pattern due to distorted growth (zones E_1, E_2). After annealing, no cathodoluminescence spectra or photograph could be obtained from Q262, as this sample broke during the annealing process. A comparison with another crystal from the same fissure shows that, with the exception of zones B and C, the same differentiation of zones is possible in the unirradiated crystal (Ramseyer, 1983).

Crystal Q312 (Mullis, 1980, 1987) shows the typical growth zonation of crystals formed in a tectonically active zone (Fig. 3b). Here again the growth was preferentially normal to the rhombohedra. After annealing, crystal Q312 showed a more homogeneous luminescence distribution with only slight differences between the previously determined zones (Fig. 3c). Zone A (strong blue) is now similar to zone C (dark gray), and only zone B (blue-gray) is clearly different. Additional spectroscopic measurements on Q312 revealed that after annealing the luminescence intensity increased by a factor of 4 (Fig. 4). The peak positions in the spectra, however, were not affected. The difference between the bluish (A_4^2) and blue-green luminescing part (B_4^2–B_4^3) is due to the difference in the intensity ratio of the 390 and 480 nm peaks (Fig. 4).

Based on the patterns generated by cathodoluminescence and γ irradiation, trace element profiles traversing the different growth zones were measured with the ion microprobe. The lateral trace element distribution is given in Figure 5. The positions of the measurements are indicated in Figure 3. Several interesting features can be taken from this figure:

1. Variations in Al, Li, and Na concentrations of up to 3 (Q262) and 2 (Q312) orders of magnitude exist between adjacent growth zones of some tens of micrometers width.

2. The Li and Al concentrations are very well correlated, and Na shows somewhat similar trends.

3. A comparison with Figure 2 reveals that the trace elements are not correlated with the colors produced by γ irradiation. There are zones that have the same color intensities and quite different amounts of Li (regions 1, 2, and 3 in Fig. 1; 40–350 ppma, 3000–8000 ppma, and <5 ppma, respectively) and zones with different color intensities and the same amount of Li (regions 4, 5 in Fig. 1, 500 ppma).

4. Comparing the line scan analysis (Fig. 5) with the luminescence colors (Fig. 3), one can observe a correlation with the different color zones. For both crystals, the strong blue zones in the γ-irradiated crystals (A_1, A_2, A_3, A_4, A_4^1, A_4^2, A_4^3) show highest but different Al, Li, and Na enrichments.

Concentrations in the different luminescence zones are calculated and summarized in Table 1. For crystal Q262, the zones A–E have distinctly different Al, Li, and Na concentrations. For Q312, the situation is not so obvious. Except for the higher concentration in zones A_4, A_4^1, and A_4^2, there are several regions that can hardly be assigned to the zones B or C defined for crystal Q262. Nevertheless, there are significant color differences (B_4 and C_4, B_4^2 and C_4^1), whereas trace amounts only vary between 100–500 ppma and 20–50 ppma for Al and Li, respectively (Table 1).

Figure 6 shows the linear correlation of Al with Li. For Al concentrations between 20 and 2000 ppma, the average Li/Al elemental ratio is ~0.6 for Q262 and ~0.3 for Q312. However, in zones A_1 and A_3 of Q262, Li is as abundant as Al. Except for the four points with Al < 5 ppma, the Na concentrations are much lower than those of Li and the Li/Na elemental ratios vary between 0.0003 and 0.1. Some correlation trends of Na with Al are visible in Figure 5, but the Na/Al ratio also shows large variations. Assuming charge neutrality, i.e., $[Al^{3+}] \approx [Li^+] + [Na^+] + [H^+]$, we obtain average H/Al elemental ratios of ~0.4 for Q262 and ~0.7 for Q312.

DISCUSSION AND CONCLUSIONS

Artificial γ irradiation

In natural colorless and smoky quartz crystals, a direct relationship exists between the intensity of the artificial color and the concentration of $[AlO_4/Li^+]^0$ point defects, i.e., the concentration of Li (<100 ppma Li; for details see Bambauer, 1961). Samples Q262 and Q312 show no such relationship. The radiation-induced $[AlO_4]^0$ centers are responsible for the smoky color (Nassau, 1978; Halliburton et al., 1981; Weil, 1984). Their concentration depends on the concentration of $[AlO_4/Li^+]^0$ point defects and on the radiation dose and also on the spontaneous recombination of closely spaced electron traps and holes and on the simultaneous recombination of non-Al-associated H and $[AlO_4/Li^+]^0$ point defects during irradiation (Lipson and Kahan, 1985; Siebers, 1986). Lack of a direct relationship between the intensity of the color produced by γ irradiation at room temperature and the concentration of $[AlO_4/Li^+]^0$ point defects may thus be the result of non-Al-associated H and spontaneous recombination of electron traps and holes in areas with >100 ppm $[AlO_4]^0$

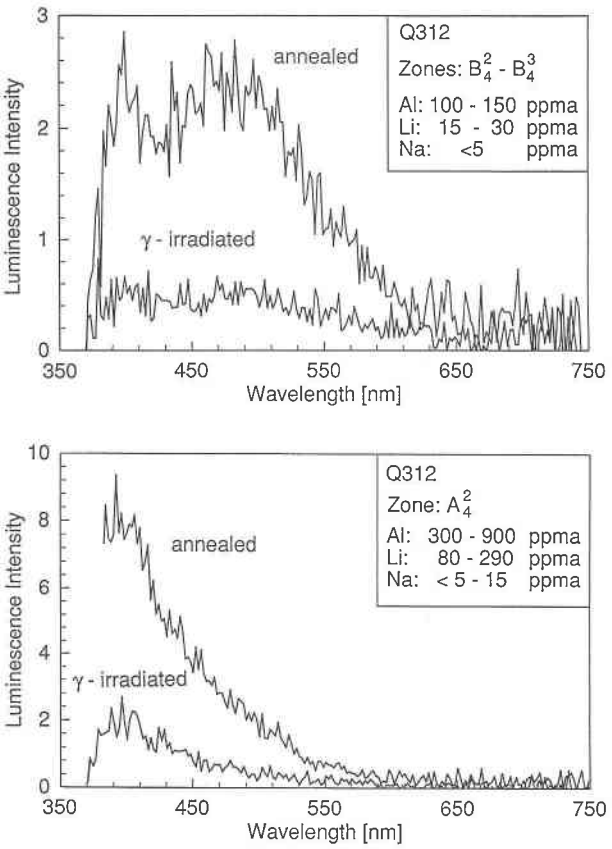

Fig. 4. Cathodoluminescence spectra taken after γ irradiation and after subsequent annealing (400 °C, 72 h) from zones B_4^2 to B_4^3 and A_4^2 in Q312.

centers (Halliburton et al., 1981; Lipson and Kahan, 1985; Siebers, 1986). For Q262 and Q312, non-Al-associated H is one likely cause as IR spectroscopy revealed the occurrence of non-Al-associated OH groups in alpine fissure quartz crystals (Bambauer et al., 1962). Spontaneous recombination of electron traps and holes in zones of >2000 ppma Al is another possible cause as these zones are only slightly colored.

Cathodoluminescence

The annealed crystal Q312, an unirradiated crystal from the same locality as Q262 (Ramseyer, 1983), and luminescence observations on the quartz crystals used for SIMS calibration revealed that zones with <5 ppma Al are nonluminescent. This value is ~20 times smaller than previously determined by electron microprobe (110 ppma Al; Ramseyer and Mullis, 1990). Annealed or unirradiated samples with >5 ppma Al always show luminescence, whereas this may not be true for irradiated specimens. A concentration dependence of the luminescence is not so obvious from Figure 3c, but spectral measurements in Q312 at positions of different trace contents show a larger peak intensity at 390 nm for the position A_4^2, with a higher trace element content (Fig. 4). As zones with higher concentrations, i.e., >2000 ppma Al, are not present in the annealed sample it is impossible to decide whether concentration quenching may occur. From these findings, Al or a specific cation-compensated Al point defect may be considered as luminescence center of the short-lived cathodoluminescence, as suggested for the blue emission in thermoluminescence, X-ray luminescence, and phosphorescence (Malik et al., 1981; Katz and Halperin, 1988; Yang and McKeever, 1990; Halperin, 1991). This hypothesis is supported by the following observations:

The observed decrease of the luminescence intensity through γ irradiation (Fig. 3) is evidence that $[AlO_4/Li^+]^0$ point defects may be likely luminescence centers of the short-lived luminescence, as $[AlO_4/Li^+]^0$ point defects decrease in concentration during γ irradiation at room temperature and can be regenerated by annealing (Jani et al., 1983; Halliburton et al., 1981; McKeever et al., 1985; Lipson and Kahan, 1985; Siebers, 1986). Further support of this hypothesis comes from the temperature dependence of the luminescence intensity, which shows a drastic increase of the intensity below 190 K, the temperature above which interstitial alkali ions can be removed by γ irradiation from the $[AlO_4/Li^+]^0$ point defects (Hanusiak and White, 1975; Halliburton et al., 1981; Halperin, 1991). In addition, from annealing experiments we know that the diffusion coefficient of the luminescence centers is similar to those of single charged ions such as H^+, Li^+, Na^+, or K^+ (Ramseyer and Mullis, 1990). Peroxy radicals or $[H_3O_4]^0$ defects, which act as luminescence centers in thermoluminescence, are unlikely candidates as these centers must first be generated by γ irradiation from precursor point defects (Griscom, 1979; Gritsenko and Lisitsyn, 1985; Yang and McKeever, 1990). In our spectra we also see no evidence at 510, 695–727, or 620 nm for luminescence activated by a transition metal or REE (i.e., Mn^{2+}, Fe^{3+} or Eu, Sm; Pott and McNicol, 1971; Hashimoto et al., 1987).

Al, Li, and Na correlation

Bulk analyses on several hundred hydrothermal quartz crystals from different localities all over the Swiss Alps demonstrated that the trace element concentrations varied from 10 to 2500 ppma (Bambauer, 1961). Over the whole concentration range, elemental Al was equal to the sum of Na, Li, and H. The Na had no pronounced correlation with Al and Li, and the concentrations never passed the limit of 40 ppma. The major charge compensating ions are therefore Li and H, and each showed a linear correlation with Al.

The Li, Al correlation from Bambauer (1961) and Poty (1969) is in excellent agreement with our data obtained from microscopic zones of single crystals. In addition, the variability in the concentration of the trace elements in Q262 is larger than the published range for ordinary rock-forming crystals and crystals composed of optically an-

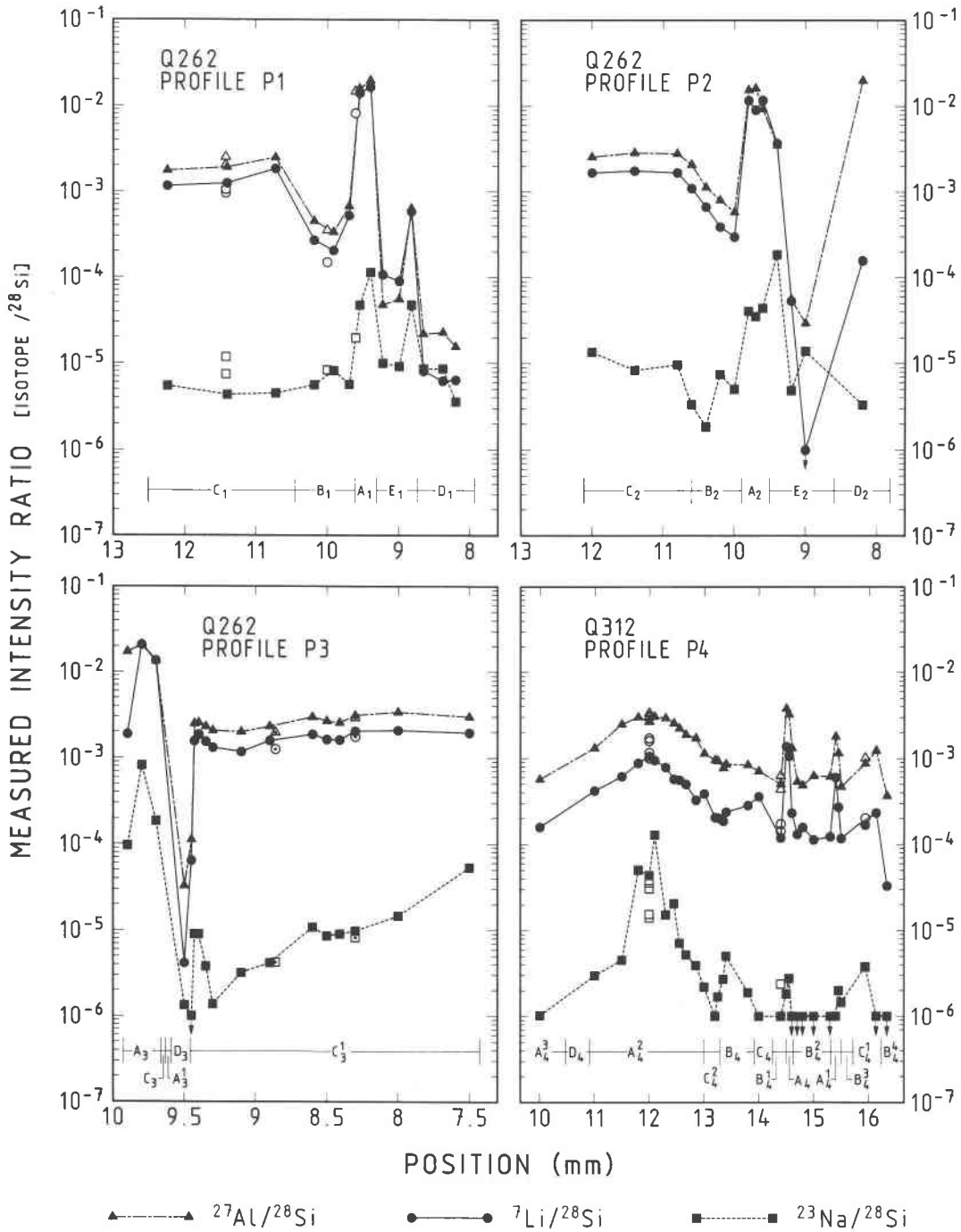

Fig. 5. Line scan analyses showing the lateral distribution of the trace elements along lines P1, P2, and P3 of sample Q262 and P4 of Q312. Each point (Fig. 3) consists of a series of single measurements with an analyzed area of 10 μm in diameter. Filled symbols represent data taken during one measuring period (~ one week); open symbols are remeasurements to check the reproducibility during a long-time period (~ six months). The symbols with a centered point in profile P3 mark the crossing with the profiles P1 and P2. Arrows mark points with values below detection limit.

isotropic domains collected from the entire Swiss Alps (Bambauer, 1961).

The difference in the inferred H concentration between Q312 and Q262 is most likely caused by the observed difference in the CO_2 concentration of the hydrothermal fluid as deduced from fluid inclusions (i.e., pH; Pankrath, 1988; Mullis, 1976, 1980).

The most surprising observation in the trace element distribution in the two analyzed crystals is the occurrence of drastic changes in the concentration of Al, Li, and Na

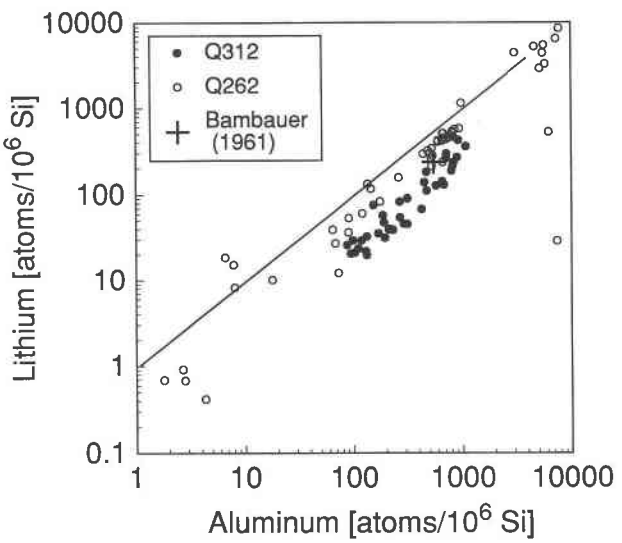

Fig. 6. Correlation plot for the trace element concentrations. Open symbols represent data from sample Q262, whereas filled symbols are values from sample Q312. The cross marks the concentrations determined by Bambauer (1961) in another crystal from the same region as Q312 (550 ppma Al, 235 ppma Li). The solid line marks equal concentrations of Al and Li.

on the scale of tens of micrometers (Fig. 5). Most likely, these concentration changes reflect differences of trace element incorporation during growth, as the concentration changes coincide with growth stages visible under cathodoluminescence (Fig. 3). An uptake after crystallization would imply diffusion of these elements into the crystal. In the case of Al, where the diffusion rate is 10^{-27} m²/s at 400 °C (Pankrath, 1988), this process is slow even at high temperatures so that diffusion through 1 μm at 400 °C would require $>10^7$ yr (Freer, 1981).

Trace element determinations in natural and in synthetic quartz crystals grown in various hydrothermal solutions containing trace elements (e.g., MOH, $MHCO_3$, M_2CO_3, or MF solutions, M = alkali element) reveal the following:

1. The addition of Al to the solution where quartz is growing substantially increases the incorporation of tetrahedrally coordinated Al and the corresponding charge-compensating alkali ions and H (Brown and Thomas, 1960; Staats and Kopp, 1974).

2. The incorporation of trace elements depends on the growth direction (Brown and Thomas, 1960; Cohen, 1960; Bambauer et al., 1961; Poty, 1969; Siebers et al., 1984; Siebers and Klapper, 1984; Siebers, 1986; Pankrath, 1988).

3. Temperature and growth speed can influence the uptake of trace elements by 1 order of magnitude (Bambauer et al., 1962; Poty, 1969; Laudise et al., 1972; Pankrath, 1988).

4. The solution chemistry (MOH, $MHCO_3$, MF) can change the uptake of the trace elements (Brown and Thomas, 1960; Siebers et al., 1984; Siebers and Klapper, 1984; Siebers, 1986; Pankrath, 1988).

Variations in trace element contents of more than 1 order of magnitude in zones grown in the same directions are therefore most likely due to changes in the fluid composition itself and are not an effect of temperature or growth speed.

The high variability can probably be understood by considering the predicted pH control of the $^{[4]}$Al concentration in aqueous solution (Merino et al., 1989). In the model of Merino et al., aqueous Al passes from octahedrally to tetrahedrally coordinated complexes over a narrow pH interval (1 pH unit) at a given temperature. The concentration of aqueous $^{[4]}$Al is a quasi-step function of pH and, according to the mass action law, the same should follow for the amount of tetrahedral Al that is incorporated in quartz that crystallizes from an aqueous solution. Additional support for this pH influence is the inferred low relative H abundance in the zones of highest trace element concentrations (>2000 ppma; see Fig. 6). Both high amounts of Al, Li, and Na as well as low H concentrations may result from crystallization in a high-pH aqueous solution according to Merino et al. (1989) and Pankrath (1988).

Acknowledgments

This research was supported by the Swiss National Science Foundation. The authors wish to thank F. Bühler and P. Hoppe for their support in the ion microprobe measurements and L. Diamond and O.W. Flörke for critical reading of the manuscript. Also, we should like to thank J. Fischer and K. Bratschi for preparing the figures and B. Grose for typing the manuscript. We thank the Deutsche Forschungsgemeinschaft for supporting crystal growth experiments and purchasing samples. The paper has greatly benefited from careful review by P.E. Brown, R.L. Hervig, and W.J. Harrison.

References cited

Bambauer, H.U. (1961) Spurenelementgehalte und γ-Farbzentren in Quarzen aus Zerrklüften der Schweizer Alpen. Schweizerische mineralogische und petrographische Mitteilungen, 41, 335–369.

Bambauer, H.U., Brunner, G.O., and Laves, F. (1961) Beobachtungen über Lamellenbau an Bergkristallen. Zeitschrift für Kristallographie, 116, 173–189.

——— (1962) Wasserstoff-Gehalte in Quarzen aus Zerrklüften der Schweizer Alpen und die Deutung ihrer regionalen Abhängigkeit. Schweizerische mineralogische und petrographische Mitteilungen, 42, 221–236.

Benninghoven, A., Rüdenauer, F.G., and Werner, H.W. (1987) Secondary ion mass spectrometry: Basic concepts, instrumental aspects, applications and trends. In P.J. Elving and J.D. Winefordner, Eds., Chemical analysis, vol. 86, 1227 p. Wiley, New York.

Brown, C.S., and Thomas, L.A. (1960) The effect of impurities on the growth of synthetic quartz. Journal of Physics and Chemistry of Solids, 13, 337–343.

Cohen, A.J. (1960) Substitutional and interstitial aluminum impurity in quartz, structure and color center interrelationships. Journal of Physics and Chemistry of Solids, 13, 321–325.

——— (1985) Amethyst color in quartz, the result of radiation protection involving iron. American Mineralogist, 70, 1180–1185.

Dennen, W.H. (1966) Stoichiometric substitution in natural quartz. Geochimica et Cosmochimica Acta, 30, 1235–1241.

Freer, R. (1981) Diffusion on silicate minerals and glasses: A data digest and guide to the literature. Contributions to Mineralogy and Petrology, 76, 440–454.

Griscom, D.L. (1979) Point defects and radiation damage processes in α-quartz. Proceedings of the 33rd Annual Symposium on Frequency Control, p. 98–109. Electronics Industries Association, Washington, DC.

Gritsenko, B.P., and Lisitsyn V.M. (1985) Intrinsic short-lived defects in quartz. Fizika Tverdogo Tela, 27, 1330–1331.

Halliburton, L.E., Koumvakalis, N., Markes, M.E., and Martin, J.J. (1981) Radiation effects in crystalline SiO_2: The role of aluminum. Journal of Applied Physics, 52, 3565–3574.

Halperin, A. (1991) Temperature dependence of X-ray induced luminescence of quartz crystals. Journal of Luminescence, 48–49, 606–610.

Hanusiak, W.M., and White, E.W. (1975) SEM cathodoluminescence for characterization of damaged and undamaged α-quartz in respirable dusts. Scanning Electron Microscopy, 1, 125–132.

Harrison, W.J., Holzwarth, W.J., Summa, L.L., and Huang, W.L. (1988) Aluminum contents of authigenic quartz: A possible indicator of paleo fluid chemistry? Geological Society of America Abstracts with Program, A391, 20.

Hashimoto, T., Yokosaka, K., and Habuki, H. (1987) Emission properties of thermoluminescence from natural quartz—Blue and red TL response to absorbed dose. Nuclear Tracks and Radiation Measurements, 13, 57–66.

Hervig, R.L., and Peacock, S.M. (1989) Implications of trace element zoning in deformed quartz from the Santa Catalina mylonite zone. Journal of Geology, 89, 343–350.

Hughes, H., Baxter, R.D., and Phillips, B. (1972) Dependence of MOS device radiation-sensitivity on oxide impurities. IEEE Transactions on Nuclear Science, NS-19, 256.

Jain, H., and Nowick, A.S. (1982) Electrical conductivity of synthetic and natural quartz crystals. Journal of Applied Physics, 53, 447–484.

Jani, M.G., Halliburton, L.E., and Kohnke, E.E. (1983) Point defects in crystalline SiO_2: Thermally stimulated luminescence above room temperature. Journal of Applied Physics, 54, 6321–6328.

Kats, A., Haven, Y., and Stevels, J.M. (1962) Hydroxyl groups in α-quartz. Physics and Chemistry of Glasses, 3, 69–75.

Katz, S., and Halperin, A. (1988) The low temperature phosphorescence and thermoluminescence of quartz crystals. Journal of Luminescence, 39, 137–143.

Kronenberg, A.K., Kirby, S.H., Aines, R.D., and Rossman, G.R. (1986) Solubility and diffusional uptake of hydrogen in quartz at high water pressure: Implications for hydrolytic weakening. Journal of Geophysical Research, 91, 12723–12744.

Laudise, R.A., Kolb, E.D., Lias, N.C., and Grudenski, E.E. (1972) The distribution constant in hydrothermal quartz growth. Growth of crystals, vol. 11, p. 359–363. Consultants Bureau, New York.

Lehmann, G., and Bambauer, H.U. (1973) Quartz crystals and their colors. Angewandte Chemie, International Edition, 12, 283–291.

Lipson, H.G., and Kahan, A. (1985) Infrared characterization of aluminum and hydrogen defect centers in irradiated quartz. Journal of Applied Physics, 58, 963–970.

Magee, C.W., and Botnick, E.M. (1981) Hydrogen depth profiling using SIMS—Problems and their solutions. Journal of Vacuum Science and Technology, 19, 47–52.

Malik, D.M., Kohnke, E.E., and Sibley, W.A. (1981) Low-temperature thermally stimulated luminescence of high quality quartz. Journal of Applied Physics, 52, 3600–3605.

McKeever, S.W.S., Chen, C.Y., and Halliburton, L.E. (1985) Point defects and pre-dose effect in natural quartz. Nuclear Tracks and Radiation Measurements, 10, 489–495.

Merino, E., Harvey, C., and Murray, H.H. (1989) Aqueous-chemical control of the tetrahedral-aluminum content of quartz, halloysite and other low-temperature silicates. Clays and Clay Minerals, 37, 135–142.

Mullis, J. (1976) Das Wachstumsmilieu der Quarzkristalle im Val d'Illiez. Schweizerische mineralogische und petrographische Mitteilungen, 56, 219–268.

——— (1980) Quarz-Kristalle aus dem Maderanertal. Lapis, 5, 19–21.

——— (1987) Fluid inclusion studies during very low-grade metamorphism. In M. Frey, Ed., Low temperature metamorphism, p. 162–199. Blackie, Glasgow.

Nassau, J.M. (1978) The origin of colors in minerals. American Mineralogist, 63, 219–229.

Nassau, J.M., and Prescott, B.E. (1975) A reinterpretation of smoky quartz. Physica Status Solidi (a), 29, 659–663.

Pankrath, R. (1988) Spurenelementeinbau in Tief-Quarz als Funktion der Wachstumsbedingungen und Umprägungen unter trockenen und hydrothermalen Bedingungen. Ph.D. thesis, Ruhr-Universität Bochum, Germany.

Pott, G.T., and McNicol, B.D. (1971) Spectroscopic study of the coordination and valence of Fe and Mn ions in and on the surface of aluminas and silicas. Discussions of the Faraday Society, 52, 121–131.

Poty, B.P. (1969) La croissance des cristaux de quartz dans les filons sur l'example du filon de La Gardette (Bourg d'Oisans) et des filons du massif du Mont Blanc. Science de la Terre, Mémoire 17.

Ramseyer, K. (1983) Bau eines Kathodenlumineszenz-Mikroskopes und Diagenese-Untersuchungen an permischen Sedimenten aus Oman. Ph.D. thesis, Universität Bern, Bern, Switzerland.

Ramseyer, K., and Mullis, J. (1990) Factors influencing short-lived blue cathodoluminescence of α-quartz. American Mineralogist, 75, 791–800.

Ramseyer, K., Baumann, J., Matter, A., and Mullis, J. (1988) Cathodoluminescence colors of α-quartz. Mineralogical Magazine, 52, 669–677.

Ramseyer, K., Fischer, J., Matter, A., Eberhardt, P., and Geiss, J. (1989) A cathodoluminescence microscope for low intensity luminescence. Journal of Sedimentary Petrology, 59, 619–622.

Ray, G., and Hart, S.R. (1982) Quantitative analysis of silicates by ion microprobe. International Journal of Mass Spectrometry and Ion Physics, 44, 231–255.

Rovetta, M.R., Blacic, J.D., Hervig, R.L., and Holloway, J.R. (1989) An experimental study of hydroxyl in quartz using infrared spectroscopy and ion microprobe techniques. Journal of Geophysical Research, 94, 5840–5850.

Schirmer, O.F. (1976) Smoky coloration of quartz caused by bound small hole polaron optical absorption. Solid State Communications, 18, 1349–1351.

Shimizu, N., Semet, M.O., and Allègre, C.B. (1978) Geochemical applications of quantitative ion-microprobe analysis. Geochimica et Cosmochimica Acta, 42, 1321–1334.

Siebers, F.B. (1986) Inhomogene Verteilung von Verunreinigungen in gezüchteten und natürlichen Quarzen als Funktion der Wachstumsbedingungen und ihr Einfluss auf kristallphysikalische Eigenschaften. Ph.D. thesis, Ruhr-Universität Bochum, Bochum, Germany.

Siebers, F.B., and Klapper, H. (1984) Zelluläres Wachstum und Verunreinigungsverteilung im Zuchtquarz, aufgezeigt mit der Röntgentopographie. Zeitschrift für Kristallographie, 167, 177–178.

Siebers, F.B., Giese, U., and Flörke, O.W. (1984) Growth of doped quartz and the anisotropy of impurity distribution. Zeitschrift für Kristallographie, 167, 189–190.

Smith, J.V., and Steele, I.M. (1984) Chemical substitution in silica polymorphs. Neues Jahrbuch für Mineralogie Abhandlungen, 3, 137–144.

Staats, P.A., and Kopp, O.C. (1974) Studies on the origin of the 3400 cm^{-1} region infrared bands of synthetic and natural α-quartz. Journal of Physics and Chemistry of Solids, 35, 1029–1033.

Steele, I.M., Hervig, R. L., Hutcheon, I.D., and Smith, J.V. (1981) Ion microprobe techniques and analyses of olivine and low Ca pyroxene. American Mineralogist, 66, 526–546.

Stevie, F.A., and Kahora, P.M. (1987) Secondary ion yield changes in Si and GaAs due to topography changes during O_2^+ or Cs^+ ion bombardment. Journal of Vacuum Science and Technology, A6, 76–80.

Weil, J.A. (1984) A review of electron spin spectroscopy and its application to the study of paramagnetic defects in crystalline quartz. Physics and Chemistry of Minerals, 10, 149–165.

Williams, P. (1985) Limits of quantitative microanalysis using secondary ion mass spectrometry. Scanning Electron Microscopy, 2, 553–561.

——— (1987) Aspects of quantitative analysis using secondary ion microanalysis. Proceedings of the Sixth International Conference on Secondary Ion Mass Spectrometry (SIMS VI), p. 261–268. Wiley, Chichester, England.

Wilson, R.G., Stevie, F.A., and Magee, C.W. (1989) Secondary ion mass spectrometry: A practical handbook for depth profiling and bulk impurity analysis. Wiley-Interscience, New York.

Yang, X.H., and McKeever, S.W.S. (1990) The pre-dose effect in crystalline quartz. Journal of Physics, D: Applied Physics, 23, 237–244.

Yurimoto, H., Kurosawa, M., and Sueno, S. (1989) Hydrogen analysis in

quartz crystals and quartz glasses by secondary ion mass spectroscopy. Geochimica et Cosmochimica Acta, 53, 751–755.

Manuscript received December 27, 1990
Manuscript accepted January 6, 1992

Appendix 1. Sample description

Natural quartz crystals

1. Q262. Hydrothermally grown crystal from an alpine fissure in Rupelian flysch sandstone, Val d'Illiez, southwestern Switzerland, cut parallel to the **c** axis (Mullis, 1976). The crystal consists of two generations, an older prismatic and a younger scepter morphology. The first generation is formed at 220–200 °C and 180–140 MPa, the second at 200–180 °C and 47–44 MPa. The crystal exhibits a zonal growth structure.

2. Q312. Hydrothermally grown crystal from an alpine fissure in the crystalline basement near Windgällenhütte, Aar Massiv, central Switzerland, cut parallel to the **c** axis (Mullis, 1980). The crystal consists of one prismatic part formed by lamellae of lower symmetry. The crystallization temperature was about 300 °C and the pressure 210 MPa.

NBS standards

SRM 615: glass, 72% SiO_2, 2% Al_2O_3.

SRM 470; K-411: glass, 54.3% SiO_2. Al determined with the electron microprobe in our laboratory: 0.026 ± 0.004% Al_2O_3.

SRM 470; K-412: glass, 45.35% SiO_2, 9.27% Al_2O_3.

Synthetic quartz samples

The following samples have been used as Al, Li, and Na standards in the concentration range <140 ppma. Absolute concentrations determined by atomic absorption spectroscopy. Accuracy ±20% for Al and ±30% for Li and Na (Pankrath, 1988) except for K170 with −50/+100% for Al, Li, and Na (Staats and Kopp, 1974).

1. Q661. Smoky quartz, optical grade, origin: unknown U.S. firm, seed cut perpendicular to **c** axis. Al, Li, Na = 77, 70, <13 ppma, respectively (Pankrath, 1988).

2. Q647. Smoky quartz, origin: USSR, seed cut perpendicular to **c** axis. Al, Li, Na = 57, 14, 48 ppma, respectively (Siebers, 1986).

3. QHAF36. Hydrothermally grown from 1.35 m NH_4F-H_2O solution, doped with Fe_2O_3 and 1 g/L LiF, growth temperature 317 °C, pressure 1.21 kbar, growth rate 0.02 mm/d, seed cut perpendicular to **c** axis. Al, Li, Na = <48, 136, <50 ppma, respectively (Siebers, 1986).

4. QHAF9. Hydrothermally grown from 3.2 m NH_4F-H_2O solution, doped with Fe_2O_3, growth temperature 405 °C, pressure 1.75 kbar, growth rate 0.28 mm/d, seed cut parallel to **c** axis. Al, Li, Na = 8, 10, <20 ppma, respectively (Siebers, 1986).

5. Q659. Optical grade, G shape, origin: Sawyer Research, U.S.A.; seed cut parallel to **c** axis. Al, Li, Na = 8, 7, <13 ppma, respectively (Siebers, 1986).

6. K170. Hydrothermally grown from 0.5 N RbOH solution without dopant, growth temperature 460 °C, pressure 1.2 kbar, seed cut parallel to **c** axis. Al, Li, Na = 67, 17, 13 ppma, respectively (Staats and Kopp, 1974).